Am J Transl Res 2026;18(5):4410-4419
www.ajtr.org /ISSN:1943-8141/AJTR0171126

Original Article

Downregulation of miR-130b-3p is associated with the progression of type 2 diabetic nephropathy

Xukai Hua[1,2], Xiaoyan Zhu[2], Jianzhuo Wu[3], Hongbin Zhang[4]

[1]The First School of Clinical Medicine, Southern Medical University, Guangzhou, Guangdong, China; [2]Department of Laboratory, Foresea Life Insurance Guangzhou General Hospital, Guangzhou, Guangdong, China; [3]Xiaolan People's Hospital of Zhongshan, Zhongshan, Guangdong, China; [4]Basic Laboratory of General Hospital of Southern Theater Command, Guangzhou, Guangdong, China

Received December 30, 2025; Accepted April 8, 2026; Epub May 15, 2026; Published May 30, 2026

Abstract: Objective: To investigate the association between miR-130b-3p and the progression of type 2 diabetic nephropathy (T2DN) and the underlying mechanisms. Methods: A total of 279 patients with T2DN were enrolled and divided into the normal albuminuria (NAU) group (n=117), microalbuminuria (MIAU) group (n=98), and the macroalbuminuria (MAAU) group (n=64). Additionally, 80 healthy subjects were selected as the control group. The expression of miR-130b-3p was measured in each group, and the clinical biochemical parameters were recorded. A diabetic nephropathy (DN) rat model was established to further analyze the relationship between miR-130b-3p expression and the Bcl-2/Bax pathway. Results: The relative expression level of miR-130b-3p was significantly decreased in patients with type 2 diabetic nephropathy (T2DN). Moreover, its expression in patients of the MAAU group was notably lower than that in patients of the MIAU group. miR-130b-3p in T2DN patients was substantially negatively correlated with the course of disease, HbA1c, HOMA-IR, triglycerides, eGFR, TGF-β1 and TNF-α. Receiver operating characteristic (ROC) curve analysis demonstrated the diagnostic value of miR-130-3p for DN, with an area under the curve (AUC) of 0.854. Compared with the control group, the expression of miR-130b-3p and Bcl-2 in renal tissues of rats in the DN model group was significantly decreased, while the expression of Bax and caspase-3 was significantly increased. Additionally, the number of apoptotic cells in the renal cortex of rats in the DN model group was significantly higher than that in the control group. Conclusion: Downregulation of miR-130b-3p in T2DN patients may reflect early renal injury in DN. Its underlying mechanism may involve the induction of apoptosis through the mitochondrial pathway activation, mediated by Bcl-2/Bax imbalance.

Keywords: miR-130b-3p, type 2 diabetes mellitus, diabetic nephropathy, disease progression, mechanism

Introduction

Diabetes mellitus (DM) is a chronic endocrine and metabolic disorder characterized by persistent hyperglycemia. Patients with DM commonly exhibit disturbances in glucose and lipid metabolism. Current evidence indicates that DM arises from complex interactions between genetic predisposition and environmental factors [1]. As a lifelong condition, chronic hyperglycemia in DM drives progressive structural damage and functional impairment across multiple organ systems. Diabetic microvascular complications-including retinopathy, nephropathy, and peripheral neuropathy-are major contributors to morbidity and mortality [2].

Diabetic nephropathy (DN), defined as kidney injury resulting from sustained hyperglycemia, can affect all renal compartments, including glomeruli, tubules, interstitium, and vasculature. Notably, DN has surpassed primary glomerulonephritis as the leading cause of end-stage renal disease (ESRD) in China [3]. Despite extensive investigation, the precise etiology and pathogenesis of DN remain incompletely elucidated. It is widely accepted that DN develops through multifactorial mechanisms, likely involving the interplay between genetic susceptibility and modifiable risk factors-such as intraglomerular hypertension, hyperglycemia-induced metabolic dysregulation (e.g., oxidative stress, advanced glycation end-product accu-

https://doi.org/10.62347/JLDI4762

mulation), systemic hypertension, and dysregulation of vasoactive mediators [4].

MicroRNAs (miRNAs) are highly conserved, endogenous, noncoding RNAs approximately 22 nucleotides in length. They function as critical post-transcriptional regulators of gene expression and profoundly influence cellular processes, including proliferation, apoptosis, and differentiation [5]. Accumulating evidence confirms tissue-specific miRNA expression in the kidney, and dynamic changes in miRNA profiles are closely associated with renal functional decline, highlighting their potential utility as diagnostic and prognostic biomarkers for kidney diseases [6].

Importantly, high-throughput profiling studies have consistently identified aberrant expression of miR-130b-3p in patients with various forms of nephropathy, suggesting its involvement in renal injury pathways [7]. Building upon these findings, the present study aimed to investigate the clinical relevance and mechanistic role of miR-130b-3p in type 2 diabetic nephropathy (T2DN), with a particular focus on its association with disease progression and underlying molecular mechanisms.

Materials and methods

Clinical data

A total of 279 T2DN patients hospitalized during June 2023 and June 2025 were retrospectively included in this study. The patients were classified into three groups according to the urinary albumin-to-creatinine ratio (UACR): normoalbuminuria group (NAU; UACR<30 mg/g, n=117), microalbuminuria group (MIAU; UACR: 30-300 mg/g, n=98), and marcoalbuminuria group (MAAU; UACR>300 mg/g, n=64). In addition, another 80 individuals undergoing routine health examinations during the same period were enrolled as the control group. This study was approved by the Ethics Committee of our hospital.

Inclusion and exclusion criteria

Inclusion criteria: (1) Patients diagnosed with T2DM according to the 1999 World Health Organization criteria; (2) Age between 18 and 65 years; (3) No use of medications affecting urinary albumin excretion, such as angiotensin-converting enzyme inhibitors (ACEIs) and/or angiotensin receptor blockers (ARBs); (4) Absence of other metabolic diseases other than T2DM; (5) No history of infection within one month before treatment.

Exclusion criteria: (1) Presence of hypertension, cardiovascular disease, hematological disease, malignancy, or liver disease; (2) Coexisting renal disease other than DN, urinary system disease, or chronic inflammatory disease; (3) Male patients with prostate disease; or (4) Female patients in pregnancy or lactation.

Clinical research methods

Routine laboratory measurements: Fasting venous blood samples were collected from all participants in the early morning. Parameters measured included fasting blood glucose, blood lipid, glycated hemoglobin (HbA1c), blood urea nitrogen (BUN), serum creatinine (Scr), fasting insulin, and C-peptide.

Blood samples were processed by a two-step centrifugation protocol. First, samples were centrifuged at 4°C and 1,000× g for 15 min, and the supernatant was collected. Subsequently, the supernatant was centrifuged again at 4°C, 2,000× g for 5 min, and the residual cellular debris in the serum were removed. The collected serum samples were stored at -80°C until analysis. Insulin resistance was assessed using the homeostasis model assessment of insulin resistance (HOMA-IR), calculated as: fasting insulin (mIU/L) × fasting glucose (mmol/L)/22.5. Estimated glomerular filtration rate (eGFR) was calculated using the Modification of Diet in Renal Disease (MDRD) formula: eGFR [ml·min-1·1.73m-2] = 186 × [Scr (mg/dl)]$^{-1.154}$ × [age]$^{-0.203}$ × (0.742 if female). The urine microalbumin was measured using a Beckman Coulter IMMAGE automatic immunoassay system (rate nephelometry). The UACR was calculated based on the corresponding urinary creatinine concentration. The final value was defined as the mean of three consecutive morning urine measurements.

Measurement of TGF-β1 and TNF-α: Serum levels of TGF-β1 and TNF-α were determined using ELISA kits (R&D Systems, USA). The assay was performed strictly according to the manufacturer's instructions.

Detection of miR-130b-3p in peripheral blood mononuclear cells (PBMCs): Approximately 3 ml of fasting venous blood was collected and anticoagulated with sodium heparin. Samples were centrifuged at 1,000× g for 5 min. After removing the plasma layer, an equal volume of phosphate-buffered saline (PBS) was slowly added the diluted blood was carefully layered over Ficoll density gradient medium and centrifuged at 800× g for 30 min.

The PBMC layer was collected and transferred into a new 1.5 mL EP tube, followed by centrifugation at 12,000× g for 5 min. After discarding the supernatant, 1 ml TRIzol reagent was added, and the samples were stored at -70°C until RNA extraction. Total RNA was extracted according to the instructions of the Total RNA Rapid Extraction Kit.

The real-time quantitative fluorescence PCR (QRT-PCR) was conducted on an ABI 7500 system (USA). The RNA was reverse transcribed into cDNA using a reverse transcription kit (Tiangen Biotech (Beijing) Co., Ltd.). U6 was used as the internal reference. The miRNA reverse transcription reaction system: 5 μL RNA template, 3 μL U6 and miRNA specific stem ring primers, 0.15 μL 100 mmol/L deoxy RNA (dNTPs), 1.00 μL reverse transcriptase, 1.50 μL 10× reverse transcriptase buffer, 0.19 μL RNase inhibitor, 4.16 μL sterile triple distilled water. Amplification reaction system 20 μl: 1 μl primer and probe Mix (20×), 10 μl TaqMan universal mixture solution (2×), 1.33 μl reverse transcription product cDNA, 7.67 μl nuclease-free water. The amplification conditions were as follows: pre-degenerated at 95°C for 10 mins, degenerated at 95°C for 15 s, and refolding at 60°C for 60 s, which repeated by a total of 45 rounds. The relative expression level of miR-130b-3p was calculated using the $2^{-\Delta\Delta Ct}$ method.

Animal research methods

DN mouse model: C57BL/6 mice were procured from Experimental Animal Center of Chongqing Medical University. After one week of acclimatization under standard laboratory conditions, mice were fasted for 12 h before modeling. Diabetes was induced by a single intraperitoneal injection of streptozotocin (STZ) solution (STZ dissolved in citric acid buffer solution at pH 4.5) at 150 mg/kg. Brief inhalation anesthesia with isoflurane was administered before injection to alleviate animal suffering. Blood glucose levels were measured from tail vein blood samples 72 h after STZ administration. Before blood sampling, lidocaine ointment was applied to the tail for 1 to 2 min to relieve pain. A fasting blood glucose >16.17 mmol/L indicated successful diabetes induction. The mice were fed a high-fat diet for 1 month. DN was considered successfully established when fasting blood glucose was >16.17 mmol/L and 24 h urinary protein excretion increased by more than 10-fold compared with baseline. A total of 20 mice were randomly divided into a DN model group (N=10) and a control group (N=10). The model group underwent the procedures described above, and the control group were fed normally.

Before tissue collection, mice were deeply anesthetized with isoflurane and subsequently euthanized by cervical dislocation. All experimental procedures were approved by the Animal Ethics Committee of Southern Medical University.

Detection of miR-130b-3p and apoptosis-related gene expression in mouse renal cortex: Renal cortical tissues were harvested from mice in both groups. Total RNA was extracted using Trizol reagent, and RNA concentration and purity were assessed. The RNA was reverse transcribed into cDNA using reverse transcription kit. The expression of miR-130b-3p, Bcl-2, and Bax was quantified by qRT-PCR. Primers were synthesized by Sangon Biotech (Shanghai, China), and specific sequences are shown in **Table 1**. The qRT-PCR cycling conditions were as follows: pre-denaturation at 95°C for 30 s, 95°C for 5 s, and 60°C for 35 s with a total of 40 rounds. U6 and GAPDH were used as internal reference genes. Relative expression levels were calculated using the 2^-ΔΔCt method.

Detection of apoptosis-related protein expression in mouse renal cortex by Western blot: Renal cortex tissues were harvested from both groups, minced, and lysed in RIPA buffer (Jiangsu KeyGEN BioTECH Corp., Ltd) supplemented with PMSF (Jiangsu KeyGEN BioTECH Corp., Ltd). Tissue homogenization was performed on ice for 30 min. Subsequently, the

Table 1. Primer sequence for PCR

Primer	The sequence
miR-130b-3p	Forward primer: 5'-GCCGCCGTGCAATGATGAA-3'
	Reverse primer: 5'-GTGCAGGGTCCGAGGT-3'
Bcl-2	Forward primer: 5'-TGAGGACCCAATCTGGAAACC-3'
	Reverse primer: 5'-AAACCCAAACAAATACATAAGGCAA-3'
Bax	Forward primer: 5'-CGTGGTGCCCTCTTCTACT-3'
	Reverse primer: 5'-TTGGATCCAGACAAGCAGCC-3'
U6	Forward primer: 5'-GCTTCGGCAGCACATATACTAA-3'
	Reverse primer: 5'-AACGCTTCACGAATTTGCGT-3'
GAPDH	Forward primer: 5'-ACGGATTTGGTCGTATTGGG-3'
	Reverse primer: 5'-TGATTTTGGAGGGATCTCGC-3'

homogenates were centrifuged at 12,000 g for 5 min at 4°C, and the supernatants were collected and stored at -20°C for subsequent analysis.

Protein concentration was detected using BCA method (Takara, Dalian, China). Equal amounts of protein were mixed with loading buffer and denatured by boiling for 10 min. Proteins were separated by SDS-PAGE and transferred onto polyvinylidene fluoride (PVDF) membranes. The membranes were blocked with 5% nonfat milk and incubated overnight at 4°C with primary antibodies against Bcl-2, Bax, and caspase-3 (all from Sigma, USA). After washing, membranes were incubated with appropriate secondary antibodies at 37°C for 2 h. Protein bands were visualized using enhanced chemiluminescence (ECL) reagents and detected in a darkroom. Band intensities were quantified using ImageJ software, with β-actin serving as the internal control for normalization.

Detection of apoptosis in mouse renal cortex by TUNEL: Mouse renal tissues were prepared as frozen sections, air-dried, and fixed in ice acetone for 10 min. The sections were rinsed with PBS three times. Subsequently, sections were treated with protease K working solution and incubated for 25 min at 37°C, followed by PBS washes.

Subsequently, the sections were incubated with permeabilization solution at room temperature for 20 min and washed again. The tissues were then equilibrated using equilibration buffer at room temperature for 10 min. TUNEL reaction mixture was added according to kit instruction, and the sections were incubated in a humidified chamber at 37°C for 2 hours. After washing with PBS for 3 times, the sections were counterstained with DAPI at room temperature for 10 min in dark. Finally, the sections were mounted with antifade mounting medium and observed under a fluorescence microscope. Images were captured for analysis. DAPI-positive nuclei emitted blue fluorescence, while TUNEL-positive cells exhibited green fluorescence.

Statistical analysis

Data analysis was performed using SPSS 26.0. Continuous variables are presented as mean ± standard deviation (SD). Comparison among multiple groups were performed using one-way analysis of variance (ANOVA), followed by the least significant difference (LSD) post hoc test for pairwise comparisons.

Categorical variables were expressed as frequencies and percentages, and comparisons between two groups were performed using the chi-square (χ^2) test. For non-normally distributed data or ordinal variables, the rank-sum test was applied.

The diagnostic value of miR-130b-3p in DN was analyzed using receiver operating characteristic (ROC) curve analysis. Pearson's correlation analysis was applied to assess the relationships between variables. A two-tailed *P* value *<0.05* was considered statistically significant.

Results

Comparison of baseline characteristics and clinical parameters between groups

As shown in **Table 2**, there were no significant differences in sex, age, BMI, systolic blood pressure (SBP), diastolic blood pressure (DBP), total cholesterol, low-density lipoprotein cholesterol (LDL-C), or high-density lipoprotein cholesterol (HDL-C) among the groups (*P>0.05*). The course of disease in the MAAU group was notably longer than that of the NAU group and MIAU group (*P<0.05*), whereas no significant difference was observed between the NAU and MIAU groups (P>0.05).

HbA1c, HOMA-IR, triglycerides, UACR, Scr, BUN, eGFR, TGF-β1 and TNF-α in the MAAU group

Table 2. Comparison of baseline characteristics and clinical parameters among groups ($\bar{x} \pm s$)

Parameters	Control group (n=80)	NAU group (n=117)	MIAU group (n=98)	MAAU group (n=64)	F/χ^2	P
Male (n, %)	45 (56.25)	69 (58.97)	62 (63.27)	40 (62.50)	1.116	0.773
Age (yd)	53.21±5.03	55.20±7.08	53.41±5.38	54.36±7.82	2.084	0.102
Course of disease (years)	-	4.37±1.13	4.40±1.30	5.54±1.62$^{\#,\Delta}$	18.981	0.000
BMI (kg/m^2)	25.06±2.01	25.26±2.82	24.78±2.98	24.32±2.13	1.969	0.118
Systolic blood pressure (mmHg)	119.16±10.17	121.90±11.73	120.48±12.54	122.39±11.16	1.288	0.278
Diastolic blood pressure (mmHg)	77.62±10.21	78.34±11.10	78.35±13.38	79.16±10.33	0.213	0.887
HbA1c (%)	5.30±0.44	7.33±0.43*	8.29±0.23$^{*,\#}$	8.80±0.38$^{*,\#,\Delta}$	1279.259	0.000
HOMA-IR	2.90±0.24	3.44±0.58*	3.91±0.40$^{*,\#}$	4.60±0.54$^{*,\#,\Delta}$	176.794	0.000
Total cholesterol (mmol/L)	4.25±0.93	4.48±0.70	4.59±1.13	4.65±1.26	2.408	0.067
LDL-C (mmol/L)	3.01±0.87	2.89±0.85	2.92±0.73	3.00±0.82	0.432	0.730
HDL-C (mmol/L)	1.097±0.355	1.058±0.313	1.072±0.281	1.090±0.255	0.306	0.821
triglycerides (mmol/L)	1.83±0.48	2.56±0.55*	3.41±0.68$^{*,\#}$	5.47±0.80$^{*,\#,\Delta}$	453.153	0.000
UACR (mg/g)	10.47±3.06	14.03±3.54*	68.08±11.77$^{*,\#}$	460.06±97.29$^{*,\#,\Delta}$	1911.193	0.000
Serum creatinine (μmol/L)	54.78±9.24	55.75±8.03	69.27±12.94$^{*,\#}$	108.47±19.36$^{*,\#,\Delta}$	298.540	0.000
Blood urea nitrogen (mmol/L)	5.28±0.77	5.26±1.11	5.46±1.32	7.27±1.34$^{*,\#,\Delta}$	49.964	0.000
eGFR (ml·min-1·1.73m^{-2})	126.72±16.02	129.94±19.06	115.07±15.53$^{*,\#}$	89.64±13.02$^{*,\#,\Delta}$	92.043	0.000
TGF-β1 (μg/L)	15.14±2.63	23.29±4.31*	38.35±9.54$^{*,\#}$	66.75±17.34$^{*,\#,\Delta}$	435.739	0.000
TNF-α (ng/L)	23.02±4.21	41.52±8.96*	59.09±10.70$^{*,\#}$	78.08±12.30$^{*,\#,\Delta}$	470.234	0.000

Note: BMI: body mass index; HbA1c: glycated hemoglobin; HOMA-IR: homeostasis model assessment of insulin resistance; LDL-C: low-density lipoprotein cholesterol; HDL-C: high-density lipoprotein cholesterol; UACR: urinary albumin-to-creatinine ratio; eGFR: estimated glomerular filtration rate; TGF-β1: transforming growth factor; TNF-α: tumor necrosis factor. $^{*}P<0.05$, compared with the control group; $^{\#}P<0.05$, compared with the NAU group; $^{\Delta}P<0.05$, compared with the MIAU group.

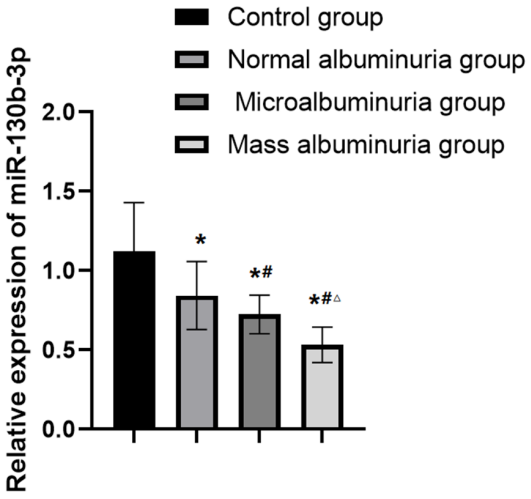

Figure 1. Comparison of miR-130b-3p expression among groups. Note: $^{*}P<0.05$, compared with the control group; $^{\#}P<0.05$, compared with the NAU group; $^{\Delta}P<0.05$, compared with the MIAU group.

were significantly higher than those in control, NAU, and MIAU groups (*P<0.05*). Similarly, HbA1c, HOMA-IR, triglycerides, UACR, Scr, eGFR, TGF-β1, TNF-α in the MIAU group were notably higher than those in control group and NAU group (*P<0.05*). In addition, HbA1c, HOMA-IR, triglycerides, UACR, TGF-β1 and TNF-α in the NAU group were significantly higher than those in control group (*P<0.05*).

Comparison of miR-130b-3p expression among groups

The relative expression level of miR-130b-3p in the MAAU group was remarkably lower than that in the MIAU, NAU, and control groups (*P<0.05*). Additionally, miR-130b-3p expression in the MIAU group was significantly lower than that in the NAU and control groups (*P<0.05*), with expression in the NAU group being significantly lower than that in the control group (*P<0.05*), as shown in **Figure 1**.

Correlation between miR-130b-3p expression and indicators of T2DN

Correlation analysis (**Figure 2**) showed no significant associations between miR-130b-3p expression and age, BMI, SBP, DBP, total cholesterol, LDL-C, HDL-C or BUN in DN patients (all *P>0.05*). However, it was significantly negatively correlated with disease duration, HbA1c, HOMA-IR, triglycerides, UACR, Scr, eGFR, TGF-β1 and TNF-α (P<0.05).

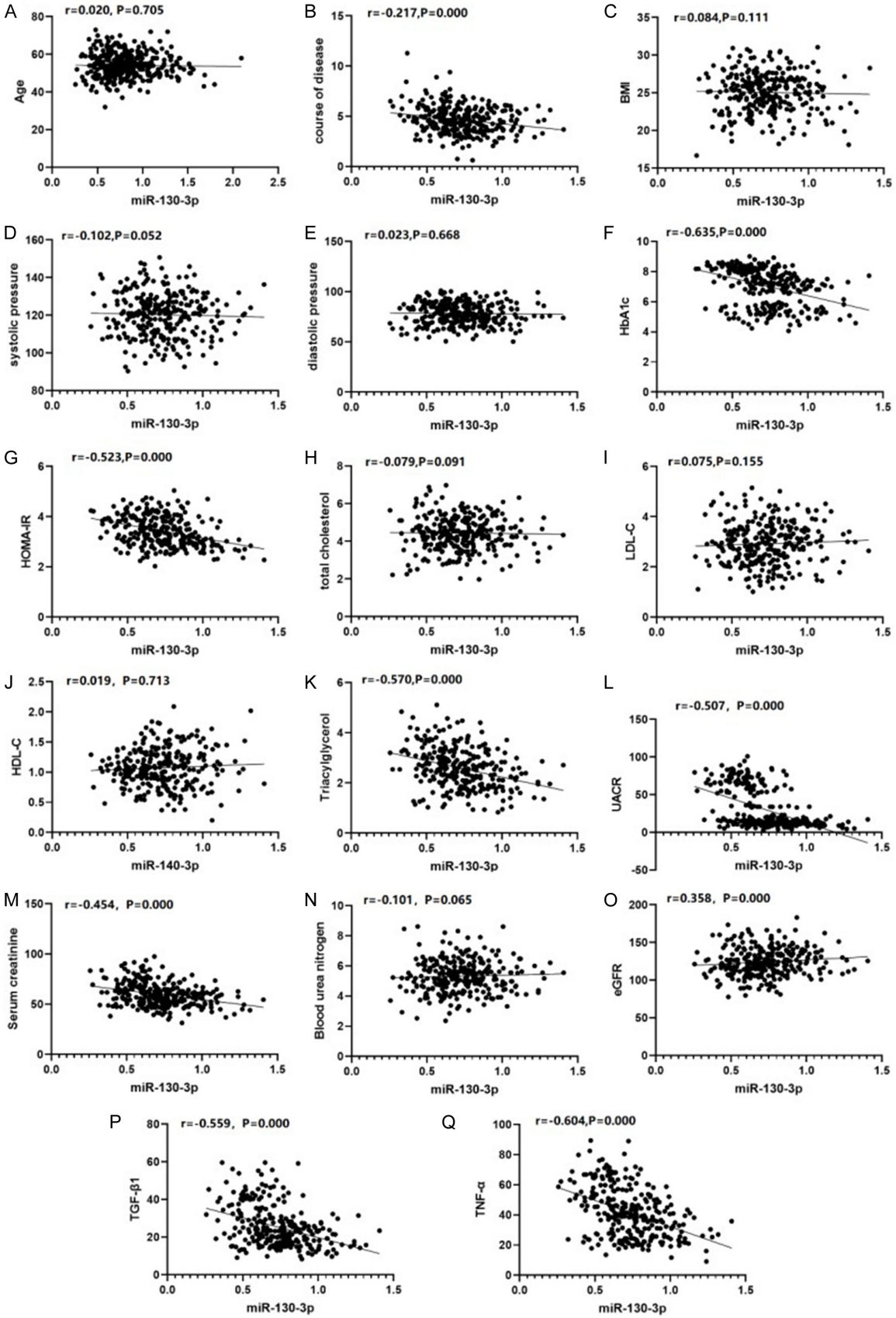
A
r=0.020, P=0.705
Age
miR-130-3p
B
r=-0.217,P=0.000
course of disease
miR-130-3p
C
r=0.084,P=0.111
BMI
miR-130-3p
D
r=-0.102,P=0.052
systolic pressure
miR-130-3p
E
r=0.023,P=0.668
diastolic pressure
miR-130-3p
F
r=-0.635,P=0.000
HbA1c
miR-130-3p
G
r=-0.523,P=0.000
HOMA-IR
miR-130-3p
H
r=-0.079,P=0.091
total cholesterol
miR-130-3p
I
r=0.075,P=0.155
LDL-C
miR-130-3p
J
r=0.019, P=0.713
HDL-C
miR-140-3p
K
r=-0.570,P=0.000
Triacylglycerol
miR-130-3p
L
r=-0.507, P=0.000
UACR
miR-130-3p
M
r=-0.454, P=0.000
Serum creatinine
miR-130-3p
N
r=-0.101, P=0.065
Blood urea nitrogen
miR-130-3p
O
r=0.358, P=0.000
eGFR
miR-130-3p
P
r=-0.559, P=0.000
TGF-β1
miR-130-3p
Q
r=-0.604,P=0.000
TNF-α
miR-130-3p

Figure 2. Scatter plot of correlation analysis. A. Correlation between age and miR-130-3p. B. Correlation between disease duration and miR-130-3p. C. Correlation between BMI and miR-130-3p. D. Correlation between SBP and miR-130-3p. E. Correlation between DBP and miR-130-3p. F. Correlation between HbA1c and miR-130-3p. G. Correlation between HOMA-IR and miR-130-3p. H. Correlation between total cholesterol and miR-130-3p. I. Correlation between LDL-C and miR-130-3p. J. Correlation between HDL-C and miR-130-3p. K. Correlation between triglycerides and miR-130-3p. L. Correlation between UACR and miR-130-3p. M. Correlation between serum creatinine and miR-130-3p. N. Correlation between blood urea nitrogen and miR-130-3p. O. Correlation between eGFR and miR-130-3p. P. Correlation between TGF-β1 and miR-130-3p. Q. Correlation between TNF-α and miR-130-3p. Notes: BMI: body mass index; HbA1c: glycated hemoglobin; HOMA-IR: homeostasis model assessment of insulin resistance; LDL-C: low-density lipoprotein cholesterol; HDL-C: high-density lipoprotein cholesterol; UACR: urinary albumin-to-creatinine ratio; eGFR: estimated glomerular filtration rate; TGF-β1: transforming growth factor; TNF-α: tumor necrosis factor.

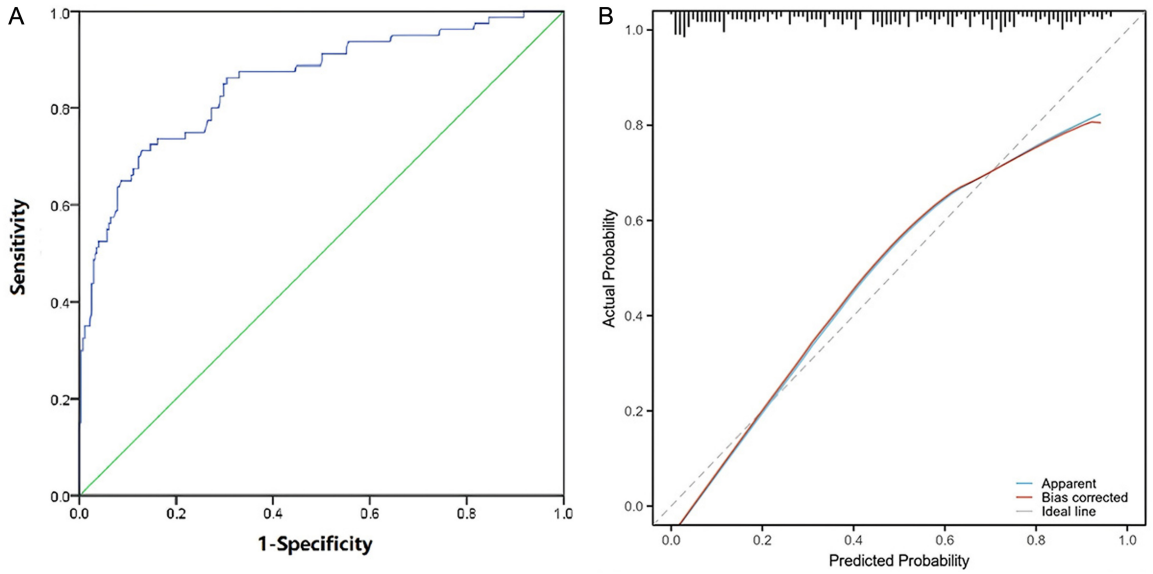

Figure 3. Diagnostic performance of miR-130b-3p for DN. A. ROC curve. B. Calibration curve. Notes: DN, diabetic nephropathy; ROC, receiver operating characteristic.

Diagnostic value of miR-130-3p for DN in diabetic patients

The diagnostic performance of miR-130-3p for DN in patients with T2DM was analyzed using ROC curve analysis. The area under curve (AUC) was 0.854 (*P<0.05*; 95% CI: 0.802-0.905) indicating good diagnostic accuracy. In addition, a calibration curve was plotted, yielding a C-index of 0.828, suggesting acceptable agreement between predicted and observed outcomes. The results are shown in **Figure 3**.

Expression and mechanistic analysis of miR-130b-3p in renal tissue of DN mice

Expression of miR-130b-3p and apoptosis-related genes: The mRNA expressions of miR-130b-3p and Bcl-2 in renal tissue of the DN group was remarkably lower than that of the control group (*P<0.05*), whereas Bax mRNA expression was significantly higher in the DN group compared with controls (*P<0.05*) (**Figure 4A**).

Expression of apoptosis-related proteins: Western blot analysis demonstrated that the protein expression of Bcl-2 was significantly decreased in the DN model group compared with the control group (*P<0.05*), whereas the protein levels of Bax and caspase-3 were notably increased (*P<0.05*) (**Figure 4B**).

Detection of apoptosis using TUNEL assay: TUNEL staining revealed that the number of apoptotic cells in the renal cortex of DN model mice was obviously higher than that in the control group (P<0.05), as shown in **Figure 4C**.

Discussion

MicroRNAs (miRNAs) are endogenous, evolutionarily conserved, single-stranded noncoding RNAs approximately 22 nucleotides in length.

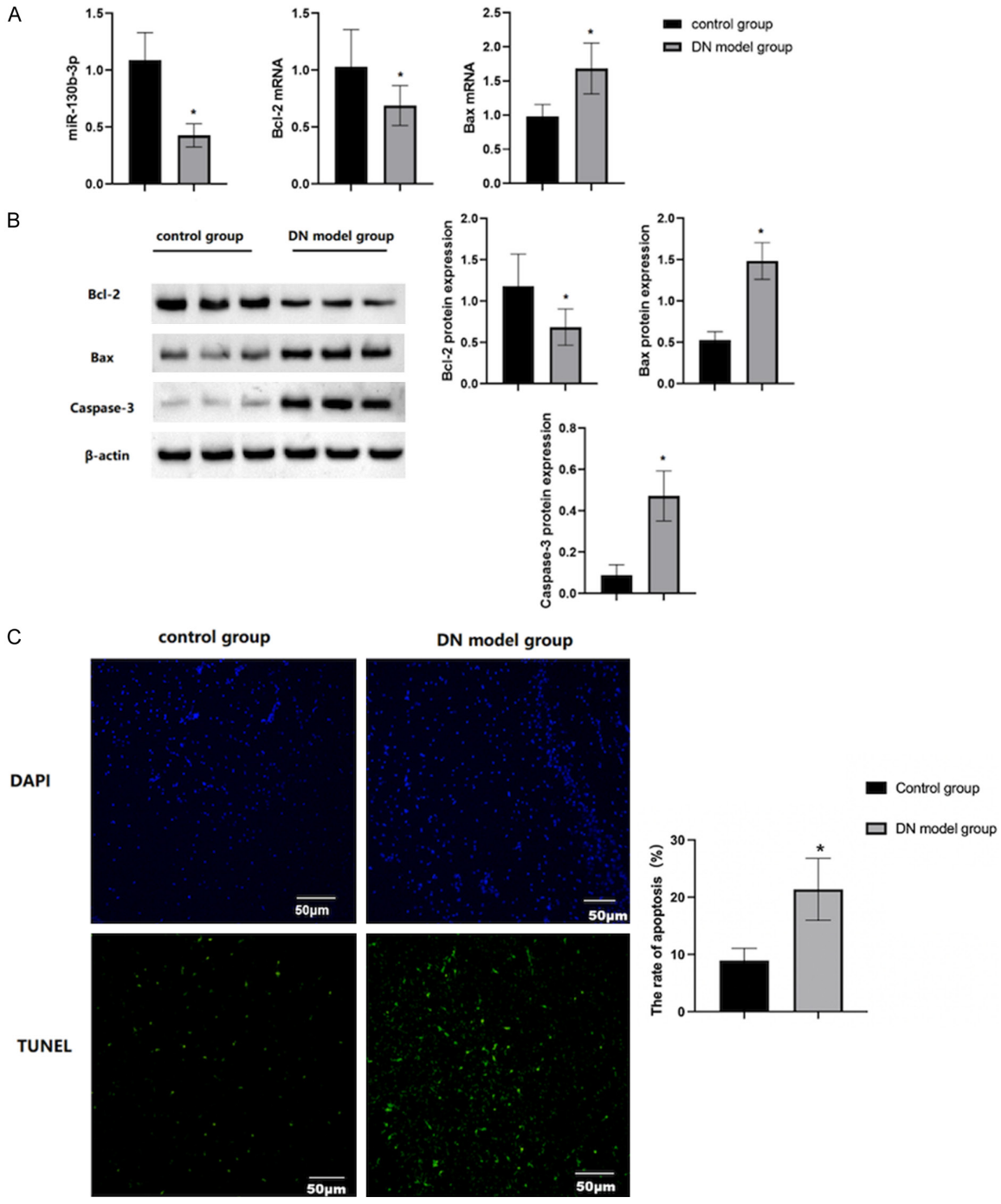

Figure 4. Expression of miR-130b-3p and apoptosis-related markers in DN mouse model. A. Relative expression of miR-130b-3p and apoptosis-related genes in the renal cortex of two groups of mice. B. Protein expression of Bcl-2, Bax and Caspase-3 in renal tissues of the two groups of mice. C. Detection of apoptosis in the renal cortex by TUNEL staining (×400). Note: $^{*}P<0.05$, compared with the control group.

They act as key post-transcriptional regulators of gene expression and play critical roles in modulating cellular processes, including cell differentiation, proliferation, and apoptosis, as well as in the initiation and progression of various pathological conditions [8-10]. Accumulating evidence has identified numerous dysregulated miRNAs in DN, many of which actively contribute to disease pathogenesis through mechanisms such as podocyte injury, mesangial expansion, tubulointerstitial fibrosis, and inflammation. Our findings substantiate

miR-130b-3p as a candidate diagnostic biomarker and therapeutic target for T2DN [11-13].

miR-130b-3p has been implicated in the regulation of diverse cellular processes, including mesenchymal cell differentiation, immune cell activation, and cellular senescence. Due to its cell- and context-specific expression and relative stability in biofluids, circulating miR-130b-3p has emerged as a promising biomarker for disease diagnosis and prognostic assessment in conditions such as obesity and hepatocellular carcinoma [14-16]. Recent evidence further links dysregulated miR-130b-3p expression to key pathogenic mechanisms in T2DM, including insulin resistance, oxidative stress, and endothelial dysfunction [17-19]. Notably, experimental evidence indicates that downregulation of miR-130b-3p in diabetic kidneys attenuates renal fibrosis-specifically by suppressing the expression of profibrotic mediators such as transforming growth factor-β receptor 1 (TGFBR1) and connective tissue growth factor (CTGF) [20-22]. Collectively, these findings strongly support a functional role for miR-130b-3p in diabetic kidney injury, positioning it as both a mechanistic mediator and a potential therapeutic target in DN.

The present study demonstrated that miR-130b-3p expression was significantly decreased across disease stages, with the lowest levels observed in the MAAU group, followed by the MIAU and NAU groups, compared with the control group. These findings suggest that miR-130b-3p is closely associated with the occurrence and progression of DN, which is consistent with previous reports [23-25]. In addition, miR-130b-3p expression in DN patients was significantly negatively correlated with the disease duration, HbA1c, HOMA-IR, triglycerides, UACR, Scr, eGFR, TGF-β1, and TNF-α. ROC curve analysis demonstrated that miR-130-3p exhibited good diagnostic performance for DN, with an AUC of 0.854. These findings suggest that miR-130b-3p may be involved in DN pathogenesis, potentially through the regulation of chronic inflammatory responses and renal fibrosis. Moreover, the decreased miR-130b-3p expression in PBMCs may reflect early renal injury in DN.

In the animal studies, the mRNA expression levels of miR-130b-3p and Bcl-2 in renal tissues of DN mice were significantly decreased compared with those in the control group, whereas the mRNA expression of Bax was significantly increased. Consistently, the protein level of Bcl-2 was reduced, while the protein levels of Bax and caspase-3 were elevated in the DN group. These alterations indicate activation of apoptosis-related pathways [26, 27]. In addition, TUNEL staining confirmed a marked increase in apoptotic cells in the renal cortex of DN mice. Collectively, these findings suggest that miR-130b-3p may exert a protective role in the kidney, and its downregulation may contribute to the progression of T2DN by promoting apoptosis. Mechanistically, this effect may be mediated through the mitochondrial apoptotic pathway involving an imbalance in the Bcl-2/Bax axis [28-30].

Conclusion

Decreased miR-130b-3p expression in T2DN patients may serve as a potential indicator of early renal injury, and its pathogenic role may be related to the induction of apoptosis via dysregulation of the mitochondrial pathway.

Disclosure of conflict of interest

None.

Address correspondence to: Hongbin Zhang, Basic Laboratory of General Hospital of Southern Theater Command, No. 111, Liuhua Road, Yuexiu District, Guangzhou 510010, Guangdong, China. Tel: +86-020-88686971; E-mail: zhangwater@hotmail.com

References

[1] Cloete L. Diabetes mellitus: an overview of the types, symptoms, complications and management. Nurs Stand 2022; 37: 61-66.

[2] Darenskaya MA, Kolesnikova LI and Kolesnikov SI. Oxidative stress: pathogenetic role in diabetes mellitus and its complications and therapeutic approaches to correction. Bull Exp Biol Med 2021; 171: 179-189.

[3] Tao L, Huang X, Xu M, Qin Z, Zhang F, Hua F, Jiang X and Wang Y. Value of circulating miRNA-21 in the diagnosis of subclinical diabetic cardiomyopathy. Mol Cell Endocrinol 2020; 518: 110944.

[4] Harreiter J and Roden M. Diabetes mellitus: definition, classification, diagnosis, screening and prevention (Update 2023). Wien Klin Wochenschr 2023; 135 Suppl 1: 7-17.

[5] Majety P, Lozada Orquera FA, Edem D and Hamdy O. Pharmacological approaches to the

prevention of type 2 diabetes mellitus. Front Endocrinol (Lausanne) 2023; 14: 1118848.
[6] Antar SA, Ashour NA, Sharaky M, Khattab M, Ashour NA, Zaid RT, Roh EJ, Elkamhawy A and Al-Karmalawy AA. Diabetes mellitus: classification, mediators, and complications; a gate to identify potential targets for the development of new effective treatments. Biomed Pharmacother 2023; 168: 115734.
[7] Sun Y, Tao Q, Wu X, Zhang L, Liu Q and Wang L. The utility of exosomes in diagnosis and therapy of diabetes mellitus and associated complications. Front Endocrinol (Lausanne) 2021; 12: 756581.
[8] Ikegami H, Hiromine Y and Noso S. Insulin-dependent diabetes mellitus in older adults: current status and future prospects. Geriatr Gerontol Int 2022; 22: 549-553.
[9] Champion ML, Battarbee AN, Biggio JR, Casey BM and Harper LM. Postpartum glucose intolerance following early gestational diabetes mellitus. Am J Obstet Gynecol MFM 2022; 4: 100609.
[10] Lambrinoudaki I, Paschou SA, Armeni E and Goulis DG. The interplay between diabetes mellitus and menopause: clinical implications. Nat Rev Endocrinol 2022; 18: 608-622.
[11] Tegegne BA, Adugna A, Yenet A, Yihunie Belay W, Yibeltal Y, Dagne A, Hibstu Teffera Z, Amare GA, Abebaw D, Tewabe H, Abebe RB and Zeleke TK. A critical review on diabetes mellitus type 1 and type 2 management approaches: from lifestyle modification to current and novel targets and therapeutic agents. Front Endocrinol (Lausanne) 2024; 15: 1440456.
[12] Esposito D, Boguszewski CL, Colao A, Fleseriu M, Gatto F, Jørgensen JOL, Ragnarsson O, Ferone D and Johannsson G. Diabetes mellitus in patients with acromegaly: pathophysiology, clinical challenges and management. Nat Rev Endocrinol 2024; 20: 541-552.
[13] Harborg S, Kjærgaard KA, Thomsen RW, Borgquist S, Cronin-Fenton D and Hjorth CF. New horizons: epidemiology of obesity, diabetes mellitus, and cancer prognosis. J Clin Endocrinol Metab 2024; 109: 924-935.
[14] Kane JP, Pullinger CR, Goldfine ID and Malloy MJ. Dyslipidemia and diabetes mellitus: Role of lipoprotein species and interrelated pathways of lipid metabolism in diabetes mellitus. Curr Opin Pharmacol 2021; 61: 21-27.
[15] Ortega HI, Udler MS, Gloyn AL and Sharp SA. Diabetes mellitus polygenic risk scores: heterogeneity and clinical translation. Nat Rev Endocrinol 2025; 21: 530-545.
[16] Lytrivi M, Tong Y, Virgilio E, Yi X and Cnop M. Diabetes mellitus and the key role of endoplasmic reticulum stress in pancreatic beta cells. Nat Rev Endocrinol 2025; 21: 546-563.
[17] Zhu B and Qu S. The relationship between diabetes mellitus and cancers and its underlying mechanisms. Front Endocrinol (Lausanne) 2022; 13: 800995.
[18] Lotti F and Maggi M. Effects of diabetes mellitus on sperm quality and fertility outcomes: clinical evidence. Andrology 2023; 11: 399-416.
[19] Singh A, Aggarwal M, Garg R, Stevens T and Chahal P. Post-pancreatitis diabetes mellitus: insight on optimal management with nutrition and lifestyle approaches. Ann Med 2022; 54: 1776-1786.
[20] Jeremiah SS, Moin ASM and Butler AE. Virus-induced diabetes mellitus: revisiting infection etiology in light of SARS-CoV-2. Metabolism 2024; 156: 155917.
[21] Rupprecht B, Stöckl A, Stöckl S and Dietrich C. Treatment of diabetes mellitus in perioperative medicine-an update. Anaesthesist 2021; 70: 451-465.
[22] Denyer AL, Catchpole B and Davison LJ; Canine Diabetes Genetics Partnership. Genetics of canine diabetes mellitus part 1: phenotypes of disease. Vet J 2021; 270: 105611.
[23] Kaur J and Seaquist ER. Hypoglycaemia in type 1 diabetes mellitus: risks and practical prevention strategies. Nat Rev Endocrinol 2023; 19: 177-186.
[24] Kietaibl AT, Huber J, Clodi M, Abrahamian H, Ludvik B and Fasching P. Position statement: surgery and diabetes mellitus (Update 2023). Wien Klin Wochenschr 2023; 135 Suppl 1: 256-271.
[25] Jagua-Gualdrón A, García-Reyes NA and Fernández-Bernal RE. Apitherapy for diabetes mellitus: mechanisms and clinical implications. J Complement Integr Med 2025; 22: 228-236.
[26] Denyer AL, Catchpole B and Davison LJ; Canine Diabetes Genetics Partnership. Genetics of canine diabetes mellitus part 2: Current understanding and future directions. Vet J 2021; 270: 105612.
[27] Tseng CH. The relationship between diabetes mellitus and gastric cancer and the potential benefits of metformin: an extensive review of the literature. Biomolecules 2021; 11: 1022.
[28] Gillery P. Biological management of diabetes mellitus, the laboratory medicine specialist and the patient. Clin Chem Lab Med 2023; 62: 1-2.
[29] Liu Y, Wang Q, Wu K, Sun Z, Tang Z, Li X and Zhang B. Anthocyanins' effects on diabetes mellitus and islet transplantation. Crit Rev Food Sci Nutr 2023; 63: 12102-12125.
[30] Dehghan M, Ghorbani F, Najafi S, Ravaei N, Karimian M, Kalhor K, Movafagh A and Mohsen Aghaei Zarch S. Progress toward molecular therapy for diabetes mellitus: a focus on targeting inflammatory factors. Diabetes Res Clin Pract 2022; 189: 109945.